LINEAR BURN RATE OF GREEN IONIC LIQUID MULTIMODE MONOPROPELLANT

BY

NICOLAS RASMONT

THESIS

Submitted in partial fulfilment of the requirements
for the degree of Master of Science in Aerospace Engineering
in the Graduate College of the
University of Illinois at Urbana-Champaign, 2019

Urbana, Illinois

Adviser:

Associate Professor Joshua L. Rovey

ABSTRACT

Multimode space propulsion systems are being proposed that integrate high specific impulse electric propulsion and high thrust chemical propulsion. The most important attribute of this concept is a shared propellant capable of both modes of propulsion, which enables mission flexibility. One promising approach is a catalytic monopropellant thruster paired with an electrospray electric thruster. Previous research has identified a green double-salt ionic liquid consisting of 41% wt. 1-ethyl-3-methylimidazolium ethyl sulfate and 59% wt. hydroxylammonium nitrate as a promising propellant candidate. In this work, the burn rate of this monopropellant is measured through pressure-based and high-speed imaging methods in a fixed-volume chamber pressurized across a pressure range from 0.5 to 10 MPa. Its performance is benchmarked by 80% wt. hydroxylammonium nitrate-water and nitromethane propellants. The burn rate of the multimode monopropellant is found to follow an exponential law given by $r_b = 5.35e^{1.11P}$ between 0.5 and 3 MPa and is approximately constant at 142 ± 29 mm/s between 3 and 10 MPa. This work was published during the AIAA Propulsion and Energy 2019 Forum: https://arc.aiaa.org/doi/10.2514/6.2019-4294. The results of this study were used to develop an improved propellant production procedure which can be found in the appendix.

ACKNOWLEDGEMENTS

First and foremost, I would like to thank my adviser Dr. Joshua L. Rovey for his continuous encouragements and support. This collaboration has been an extraordinarily formative experience and I have greatly enjoyed it. Thank you for believing in me.

I would also like to thank the current and past members of the Electric Propulsion Lab, namely Chris, Alex, Steve, Toyofumi, Hussein, Matt, Matt, and Matt, for their kindness and their help over these 18 months. Grad school would not have been the same without you. Also, thanks to my undergraduate research assistants Emil and Kentaro without whom this project would have been a lot harder to pull off in time.

Thanks a lot to the Aerospace and Civil Engineering machine shops for their help on the custom pressure vessel parts and for helping me find and operate the largest hex wrench I've ever seen. Also, huge thanks to Tom Hennessey from the UIUC Chemistry Department for his help providing lab space and equipment for propellant preparation even under short notice.

I would like to thank my family for their love and support while far away from them. Our weekly calls really helped me go through all this. Last but not least, I want to thank to Nantao for his reassurance and kind support during this past year.

TABLE OF CONTENTS

LIST OF ILLUSTRATIONS

LIST OF TABLES

NOMENCLATURE

y_i	=	Flame front position in HSI data
$\hat{y}_i$	=	Flame front position evaluated using linear regression model
n	=	HSI sample size
t_i	=	Time of acquisition of HSI datapoint
$\bar{t}$	=	Average of all acquisition times of the sample
σ_{HSI}	=	Relative error of HSI-based burn rate measurements
σ_P	=	Relative error of pressure-based burn rate measurements
r_b	=	Linear burn rate (mm/s)
D_c	=	Diameter of propellant container (mm)
V	=	Volume of propellant (mL)
Δh	=	Change in height (mm)
Δt	=	Change in time (s)
P	=	Pressure (MPa)
a	=	Burn rate coefficient (mm/s)
n	=	Burn rate exponent (unitless)

CHAPTER 1

INTRODUCTION

Multimode propulsion is defined as the integration of two distinct propulsive modes into a single propulsion system. The most important attribute is shared propellant between the propulsive modes. Recent research has focused on combining high specific impulse, low thrust electric propulsion and low specific impulse, high thrust chemical propulsion. The availability of both propulsion modes offers a high degree of flexibility during the mission design phase, by allowing trajectories and maneuvers that would be impossible otherwise[1–5]. The chemical mode is well-suited for time-sensitive maneuvers, such as orbit insertion, rendezvous or debris avoidance, while the electric mode is useful for long, high Δv maneuvers such as orbital stationkeeping and interplanetary transfer. This combination can lead to significant mass savings and shorter transfer time compared to a spacecraft equipped with a single propulsion method. Even greater mass savings can be achieved by sharing propellant and thruster hardware, even if the performance of such a hybrid system is lower in both propulsion modes than two separate specialized propulsion systems[6,7]. The use of a common propellant allows any combination of maneuvers to be realized before propellant depletion, enhancing mission flexibility. The benefits of this configuration are particularly significant for small spacecraft with mass less than 50 kg, for which the weight penalty associated with two separate propulsion systems would negate most benefits. One promising multimode architecture pairs a catalytic combustion thruster with an electric electrospray thruster sharing a common monopropellant[8–10]. Previous investigations focused on finding a suitable propellant for this application, and identified a green double-salt ionic liquid mixture of 41% 1-ethyl-3-methylimidazolium ethyl sulfate ([Emim][$EtSO_4$]) and 59% hydroxylammonium nitrate

(HAN) by mass [11]. It combines high performance in both propulsion modes with relatively low toxicity and low volatility [8,11,12].

The development of this propellant rests on the considerable advances made in electrospray propulsion in recent years[13]. This progress has been driven by the increase in small satellite launches, for which electrospray micropropulsion is particularly well-suited, as the thrust-to-power and thrust-to-weight ratios of such a system are higher than any other electric thruster technology available[14]. For this application, room-temperature ionic liquids (IL) such as [Emim][$EtSO_4$] are ideal propellants, as they have negligible vapor pressure and high electrical conductivity[15]. HAN is an ionic compound with a low vapor pressure, therefore an [Emim][$EtSO_4$]-HAN blend is a viable electrospray propellant. Previous analysis[16] showed that [Emim][$EtSO_4$] could react as a fuel with HAN as the oxidizer, with an ideal oxidizer-to-fuel (O/F) ratio of 4 (80% HAN per weight). Catalyst materials impose a limit on propellant flame temperature, which led to the current O/F ratio of 1.44 (59% HAN).

The choice of a HAN-based multimode propellant is the result of recent research efforts focused on finding a suitable replacement for legacy storable propellants. Historically, hydrazine and its derivatives have been ubiquitous in satellite propulsion systems, either alone as a monopropellant or as a bipropellant in association with nitric acid or nitrogen tetroxide. These propellants have the advantages of being easy to ignite, pose little risk of detonation, and are stable at room temperature [17]. However, their high toxicity and volatility greatly complicate handling, which increases launch costs[17–19]. Among the most promising alternatives to hydrazine currently being developed are energetic ionic compounds, namely hydroxylammonium nitrate (HAN), ammonium dinitramide (ADN) and hydrazinium nitroformate (HNF) [18,20–23]. These salts have highly

exothermic decomposition reactions, which allow them to be used as a monopropellant. They are typically blended with additives to enhance specific impulse (fuel compounds, such as methanol or ammonia) and fine tune the physicochemical properties of the propellant (glycerol to lower vapor pressure or water to adjust viscosity and flame temperature). The resulting propellants, such as AF-M315E (HAN-based, developed by the US Air Force Research Laboratory) or LMP-103S (ADN-based, developed by EURENCO-Bofors and ECAPS), have a higher specific impulse and impulse density, and lower toxicity than hydrazine[17]. Both are rapidly maturing technologies, with LMP-103S having been successfully tested on the PRISMA ESA mission in 2010 and AF-M315E tested on the Green Monopropellant Infusion Mission (GPIM) launched in June 2019 [24] [25]. However, these propellants are not usable in a multimode microtube electrospray thruster, as they contain volatile compounds that impede electrospray operation.

This paper presents the linear burn rate of [Emim][$EtSO_4$]-HAN propellant for a wide range of pressure relevant to thruster operating conditions. In addition, the linear burn rate of hydroxylammonium nitrate-water (HAN-water) and nitromethane monopropellants are measured to validate the experimental method used and compare with [Emim][$EtSO_4$]-HAN. The setup of the experiment is described in Chapter 2, and experimental results are presented in Chapter 3 and discussed in Chapter 4. The conclusions of the study are presented in Chapter 5.

CHAPTER 2

EXPERIMENTAL METHODS

The experiment described here is similar to previous studies of monopropellant linear burn rate[12,26–29]. In a constant-volume pressurized vessel, a sample of monopropellant is ignited and its burn rate calculated by measuring the pressure variation with time inside the chamber and by capturing high-speed images of the burning liquid. These two methods are both used in this work and show good agreement.

2.1 Experimental Setup

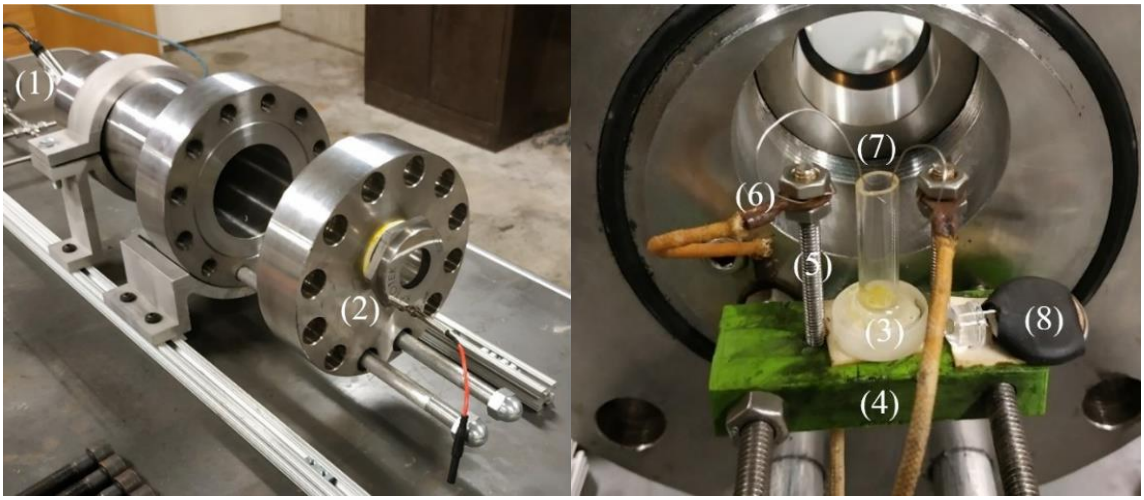

Fig. 1. Pressure vessel in open position (top) and details of the propellant holder platform (bottom).

A constant-volume pressurized vessel is used for all experiments. The vessel used for this experiment was previously used for [Emim][$EtSO_4$]-HAN burn rate experiments at a lower operating pressure[12]. It has a volume of 1.9 L, a length of 260 mm and diameter of 95.5 mm. To withstand the higher pressure of this study, a threaded section was added to the lip of the vessel,

which ensures a more robust mechanical connection between the vessel and its flange. Photographs with callouts of the components of the experimental setup are shown in Fig. 1.

Inside the pressure vessel, a sample of monopropellant is ignited and the pressure variation inside the chamber is measured with a PX309-3KG5V pressure transducer (1), with a gauge pressure range of 0 to 20.7 MPa. An ADS1115 16-bit ADC is used to acquire the sensor data with high accuracy. An SD card module piloted by an Arduino board is used to store the data. High-speed imaging (HSI) of the burn rate is performed using a Chronos 1.4 high-speed camera through a 25.4 mm viewport (2) in the flange of the pressure vessel. The propellant is held in a quartz container (3) made of a 6.02 mm-wide quartz tube epoxied to a 12.7 mm quartz disk acting as its base. The propellant is placed on a platform (4) including two threaded rods (5) acting as electrical connectors (6) for the ignition wire (7), as shown in Fig. 1. Ignition is achieved using a 28-gauge diameter nichrome wire dipped in the propellant; for some low-pressure tests, a slug of nitrocellulose (flash paper) is added to increase ignition energy. An LED (8) located inside the pressure vessel illuminates the sample. The pressurant gas is either dry nitrogen for HAN-based propellants or compressed air for nitromethane because incandescent wire ignition of nitromethane in an inert atmosphere has been shown experimentally to be difficult[26–28].

The experimental procedure starts with filling the sample holder with 0.60 mL of propellant using a graduated pipette and securing it on its platform with adhesive tape. A 70-mm-long piece of nichrome wire is cut and its extremities looped around the electrical connector columns. The wire is submerged in the propellant no more than 5% of the total liquid height. The flange is closed and secured to the vessel, and the gas cylinder regulator is set at the desired experimental pressure. The pressurization valve is opened under remote control until the pressure in the chamber stabilizes

at the desired level. A BK Precision 1665 power supply is then used to apply a 10A current through the nichrome wire, resistively heating it to a glow until rupture, triggering the ignition of the propellant. Following each test, the combustion gases are vented outside of the laboratory and the experiment can be repeated.

Three different types of propellants were tested. A formulation of [Emim][$EtSO_4$]-HAN propellant with a HAN mass concentration of 59%, the current multimode propellant blend, as well as two benchmarks: a HAN-water solution at a concentration of 80% wt. and nitromethane. These propellants were selected because of their well-explored burn rate behavior[11,26–29] and because they cover the entire range of burn rate (1-400 mm/s) that is expected for HAN-based propellants over the considered pressure domain. HAN-based propellants were manufactured from a commercial 24% by wt. HAN aqueous solution from Sigma-Aldrich with a purity above 99.999%. The solution was first concentrated up to 90% in a rotary evaporator, and the remaining water was eliminated through azeotropic vacuum distillation with isopropyl alcohol, resulting in solid HAN crystals. The crystals were then dissolved in the solvent (distilled water or [Emim][$EtSO_4$]) at the desired concentration. This method is an improvement on previously used synthesis processes [11,16], because it is more reliable and can be used with larger batches. The [Emim][$EtSO_4$] used for this study was sourced from Sigma-Aldrich with a purity above 95%. The nitromethane was also sourced from Sigma-Aldrich with a purity guaranteed above 98.5%. The pressure range for this study is 0.5 to 11 MPa. The lower part of this range, from 0.5 to 1.5 MPa, is relevant to micropropulsion operation, while the upper part up to 11 MPa provides comparison of our results with burn rate data from the literature.

2.2 Visual Measurements

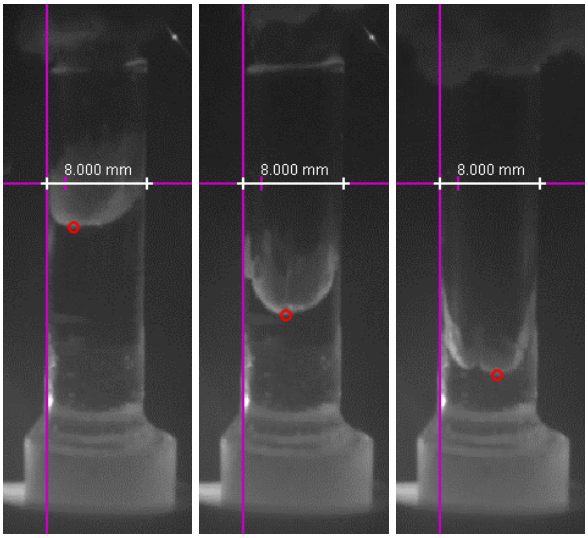

Fig. 2. Left to right: position of the decomposition front at t=0 ms, t=21.76 ms, and t=35.00 ms.

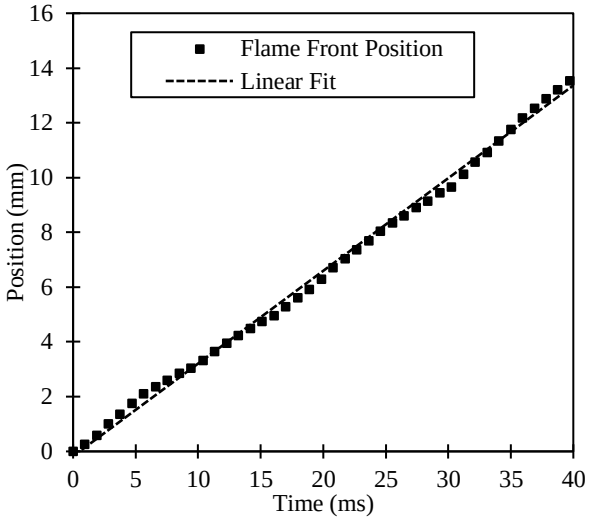

Fig 3. Data resulting from measurements presented in Fig. 2.

High-speed imaging (HSI) provides the height of propellant at any point during the combustion by comparing it with the known external diameter of the propellant holder (8.00 mm). A Chronos 1.4 high speed camera is used to acquire high-speed (1057 fps) images of the combustion. Knowing the acquisition speed of the camera, the position of the flame front in the holder during the combustion can be plotted as a function of time, and the linear burn rate is defined as the slope of the linear regression of the dataset. An example of how burn rate is determined from HSI for HAN-water propellant is shown in Fig. 2 and Fig **3**.

The standard error of the burn rate is calculated using equation (1), which is the definition of the error of the slope of a linear regression, assuming normally distributed error terms on the position datapoints.

$$\sigma_{HSI} = \sqrt{\frac{\frac{1}{n-2}\sum_{i=1}^{n}(y_i - \hat{y}_i)^2}{\sum_{i=1}^{n}(t_i - \bar{t})^2}} \quad (1)$$

The main error sources are the resolution of the camera and rapid fluctuations of the burn rate, with the latter becoming the dominant term for HAN-based propellants exhibiting unstable combustion at low pressure.

2.3 Pressure measurements

The temporal evolution of the pressure in the vessel is also used to estimate the propellant burn rate. Assuming a constant burn rate during the combustion and a uniform cross-section in the holder, the burn rate is expressed as the ratio between the change in propellant level in the holder over the burn time, as given in equation (2). This method was used in previous studies[12,28]. The height of propellant is deduced from the volume of propellant inserted in the holder. Knowing the

internal diameter of the holder, the height of propellant can be calculated. The burn time is deduced by measuring the duration of the pressure rise in the chamber from pressure sensor data.

$$r_b = \frac{\Delta h}{\Delta t} = \frac{4V}{\pi {D_c}^2 \Delta t} \tag{2}$$

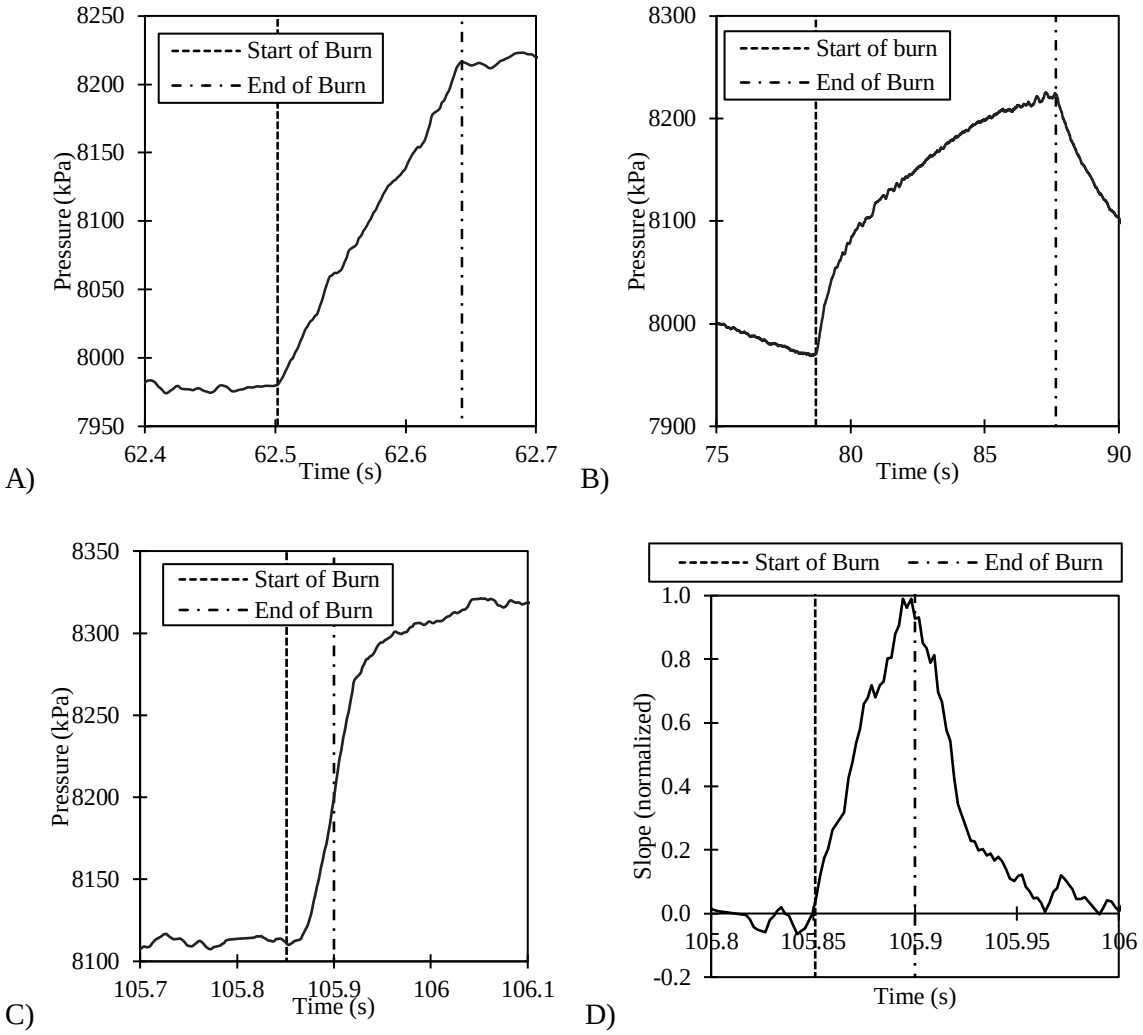

Fig. 4. Example pressure traces for (A) [Emim][$EtSO_4$]-HAN, (B) Nitromethane, and (C) 80% wt. HAN-water, and (D) slope of the pressure trace for 80% wt. HAN-water

A sliding-average filter is used to smooth the signal, with the number of samples adapted to the ignition time scale. The method used to determine the burn time depends on type of propellant studied. Nitromethane and [Emim][$EtSO_4$]-HAN pressure traces show a distinct change of slope at the beginning and end of the combustion, as seen in Fig. 4A and Fig. 4B, respectively. On the other hand, the pressure trace of HAN-water propellants continues to increase even after all the liquid propellant in the sample holder has been depleted. This behavior was documented by Stahl [28], who showed that the duration of the combustion can be accessed by taking the derivative of the pressure trace. The burn time can be calculated as the time it takes for the pressure trace slope to rise from zero to its maximum, as shown in Fig. 4C and Fig. 4D. Burn rates calculated with this method show close agreement with HSI data.

The relative uncertainty of this method, due to the compounded errors on volume and burn time measurement, decreases when the burn time increases, with a maximum of 18.2% for a burn rate of 637 mm/s and a minimum of 7.3% for a burn rate of 0.63 mm/s. The uncertainty is calculated by propagating the error from the terms present in equation (2).

$$\sigma_P = \frac{\delta r_b}{r_b} = \sqrt{\left(\frac{\delta t}{\Delta t}\right)^2 + \left(\frac{\delta V}{V}\right)^2 + 2\left(\frac{\delta D_c}{D_c}\right)^2} \tag{3}$$

The burn time error δt is due to the resolution of the pressure sensor: depending on the shape of the pressure trace, it can range from 5 to 100 ms. The volumetric error δV is due to the precision of the pipette used, which has an accuracy of ±0.01 mL. Finally, the sample holder diameter error $\delta D_c = 0.3$ mm is due to inaccuracies in the propellant holder internal geometry, which is not perfectly cylindrical due the presence of epoxy resin at its base.

CHAPTER 3

RESULTS

HAN-based propellant burn rates were acquired at pressures of 0.5, 0.75, 1.0, 1.25, 1.5, 2.0, 3.0, 4.0, 6.0, 8.0 and 10.0 MPa. Previous studies have shown that nitromethane combustion is difficult to sustain under 3 MPa [27][28], so the burn rate of nitromethane was acquired at pressures at and above 3 MPa, specifically 3.0, 4.0, 5.0, 6.0, 7.0, 8.0, 9.0, 10.0, and 11.0 MPa. Three tests at each pressure level allow the calculation of averages, 95% confidence intervals, and associated margins of error. Error bars representing measurement uncertainties are not included in the plots, as they would be smaller than the data markers themselves and thus invisible in most cases. Instead, the errors are provided as ± on values reported in the text.

3.1 Nitromethane Linear Burn Rate

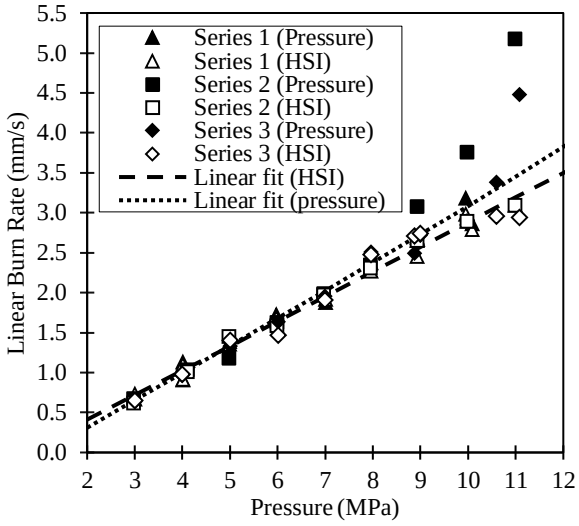

Fig. 5. Nitromethane linear burn rate results

The calculated burn rates for pressure and HSI data are presented in Fig. 5 for nitromethane. It is observed that at high pressure (>9.0 MPa), pressure-based burn rate measurements are systematically higher than HSI-based measurements. This can be explained by the increased burn rate of nitromethane during its violent ignition sequence, which skews the overall burn rate measured by pressure-based method toward higher values than the steady-state burn rate measured by HSI. This effect was not observed for HAN-based propellants, likely because of their lower ignition energy compared to nitromethane. At the lowest pressure investigated here, 3 MPa, the HSI-based burn rate was 0.67±0.05 mm/s against a pressure-based measurement of 0.66±0.02 mm/s. The relative gap between these measurements is 1.5%, within the 95% confidence interval. At the largest pressure of 11 MPa, the HSI-based burn rate was 3.05±0.09 mm/s while the pressure-based measurement was 4.35±0.85 mm/s, a 42% gap. The average margins of error of HSI and pressure-based measurements are 4.47% and 7.29%, respectively. A strong linear relationship between HSI measurements and pressure is observed over the entire range, with a coefficient of determination of 0.984 for $r_b = 0.308P - 0.208$. Similarly, pressure-based burn rates follow a law $r_b = 0.341P - 0.378$ with a coefficient of determination of 0.991 in the 3.0 to 8.0 MPa range where a linear behavior is observed.

As seen in Fig. 6, the combustion of nitromethane is laminar and exhibits a bright flame. No meniscus or bubble formation are observed. At the mouth of the propellant holder, an unstable flame is observed due to the combustion of decomposition products with oxygen. This does not impact the steady-state burn rate of nitromethane, which is due only to nitromethane decomposition and thus applicable in the context of a monopropellant.

Fig. 6. High-speed images of nitromethane decomposition

3.2 HAN-water Propellant Linear Burn Rate

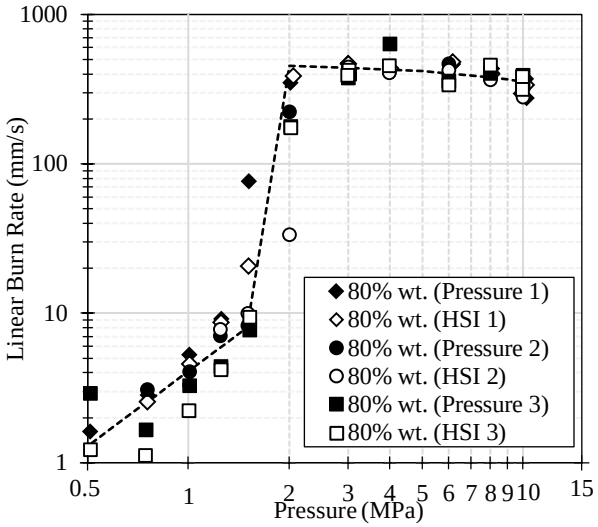

Fig. 7. 80% HAN-water linear burn rate results

HAN-water burn rate results are shown in Fig. 7 and will be discussed first, followed by discussion of the correlation of the burn rate data with visual observations of the decomposing

liquid, gas, and interface. HAN-water burn rate varies between 1-2 mm/s at low pressure (0.5 MPa) and 400-500 mm/s at higher pressure (3.0-10.0 MPa).Three burn rate regions are identified in Fig. 7: low burn rate, high burn rate, and a transition region from low to high burn rate. These regions appear to correspond with different combustion behaviors.

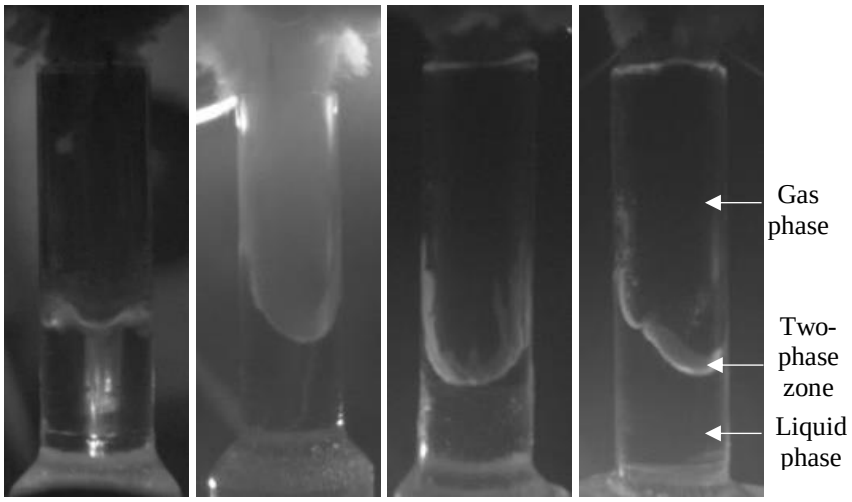

Fig. 8. Combustion structure of 80% wt. HAN-water at 1.0, 3.0, 6.0 and 10.0 MPa (left to right)

In the low burn rate region below 1.5 MPa, the burn rate shows good fit against a power law $r_b = 4.09P^{1.66}$, with a coefficient of determination of 0.74. In the high burn rate region above 3.0 MPa, the burn rate follows a slightly decreasing linear trend $r_b = 478 - 12.30P$ with a coefficient of determination of 0.365. Good agreement between HSI and pressure-based burn rate data is observed in these regions, with a maximum difference of 16% and an average difference of only 7%. Also in these regions, the margin of error is small, with a maximum of 24% in the 0.75-1.25 MPa range and 14% between 3.0 and 10.0 MPa. At 0.5 MPa the combustion is highly unstable and generates a large amount of smoke, which prevented the collection of 3 datapoints for both pressure and HSI measurements−consequently, the margin of error is larger at 44%. The transition region

is observed between 1.5 and 3.0 MPa. The margin of error within the transition region is much larger at 92%. This may be because the transition from low to high burn rate is triggered by random local disturbances in the interface between the liquid and two-phase interface, which can greatly impact the overall burn rate, as described below.

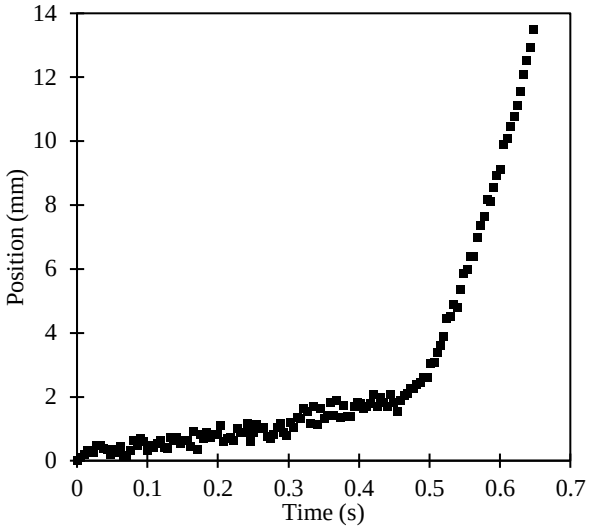

Fig. 9. Position of the burning front for 80% wt. HAN-water at 1.5 MPa showing the transition between low and high burning rate within a single test.

Each burn rate region corresponds to a different combustion behavior observed by HSI. As shown in Fig. 8, the low burn rate region presents a stratified combustion structure, with a liquid phase, a two-phase area, and an opaque gas phase. The two-phase area is thin with large bubbles being formed, resulting in an unstable interface with variable shape. The high burn rate region at higher pressure appears to have a two-phase zone with many small bubbles, as shown in Fig. 8. The interface between the liquid phase and the two-phase area is stable and adopts a curved profile, while the interface between the gas and two-phase area is unstable. High-speed images indicate that the thickness of the two-phase area decreases when pressure increases, as shown in Fig. 8.

Unfortunately, the rapidly changing gas interface does not allow for measurement of two-phase area thickness. At the lower end of the high burn rate pressure range, no interface between the gas and two-phase area was observed. In the transition region, both low and high burn rates can be observed in the same burn event, as shown in Fig. 9. The data obtained for pressures of 1.5 and 2.0 MPa corresponding to the transition region are plotted in Table 1, with the burn rates and durations being presented separately. When only one burn rate is present, the cells corresponding to the absent burn rate are dashed. Significant variability is observed in this behavior, with tests carried out at the same pressure yielding very different results: from no transition to an abrupt increase in burn rate occurring at a range of different times during the combustion. The average burn rate in the low burn rate phase is 6.32 mm/s with a margin of error of 34%. On the other hand, the high burn rate phase displays a wide variation ranging between 12.78 mm/s and 387 mm/s with an average of 156 mm/s and a margin of error of 74%.

Table 1. Burn rate data of the transition region.

Series	Pressure (MPa)	Low Burn Rate Phase		High Burn Rate Phase		Average burn rate (mm/s)
		Duration (ms)	Burn Rate (mm/s)	Duration (ms)	Burn Rate (mm/s)	
1	1.52	497	5.21	151	71.94	20.76
	2.06	-	-	31	387	387
2	1.51	1059	10	-	-	10
	2.01	343	4.73	98	134.84	33.64
3	1.53	823	5.32	1021	12.78	9.45
	2.03	-	-	80	173	173

3.3 [Emim][EtSO4]-HAN Linear Burn Rate

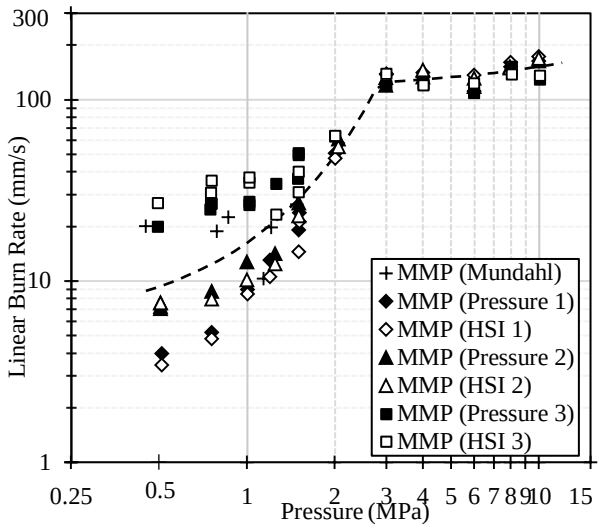

Fig. 10. Linear burn rate of 59%HAN-41%[Emim][$EtSO_4$]

The burn rate of 59%HAN-41%[Emim][$EtSO_4$] propellant is presented in Fig. 10, along with data from Mundahl et al. [12], who also investigated this propellant. A low-to-high burn rate transition is observed between 0.5 and 3.0 MPa, and an approximately constant burn rate of 142 ± 29 mm/s is observed at the high end (3.0-10.0 MPa) of the pressure range. There is no abrupt change in slope during the transition. There is good agreement between the HSI and pressure measurements in the 2.0-10.0 MPa range, with a maximum relative error of 5%. There is significant spread in the data in the 0.5-1.5 MPa range, increasing as pressure decreases, with a maximum margin of error of 54% for 0.5 MPa and an average of 21% for the entire range. This variation is not entirely random. It is due to the higher burn rates measured for one of the three test series (Series 3), while the other two test series show better agreement between each other. The average burn rate of Series 3 between 0.5 and 1.5 MPa is 32.32 ± 2.03 mm/s, while Series 1 and 2

average to 11.74 ± 1.38 mm/s. The reason behind this difference is not fully understood. It may be possible that variations during the preparation of the propellant could be the cause, as Series 3 data were acquired using a different batch of propellant. Previous measurements of linear burn rate by Mundahl [12] lie between the values of Series 3 and Series 1 and 2, without fitting well with either. The average relative difference between pressure and HSI measurement is 15% with a larger difference observed at low pressure (<2.0 MPa) likely due to smoke interference, which obscures the HSI and thus prevents the burn rate from being measured during the entirety of the burn. In the 0.5-3.0 MPa range, the data show good agreement with an exponential model, exhibiting a coefficient of determination of 0.625 for $r_b = 5.35e^{1.11P}$. When considering Series 1 and 2 only, the correlation increases to 0.934 for$r_b = 2.63e^{1.37P}$. Between 3.0 and 10.0 MPa, a slightly increasing linear trend is observed, with a correlation of 0.315 for $r_b = 3.84P + 114$. For Series 1 and 2 only, a better fit is observed for a polynomial expression $r_b = 1.482P^2 - 14.67P + 168$ with a coefficient of correlation of 0.722.

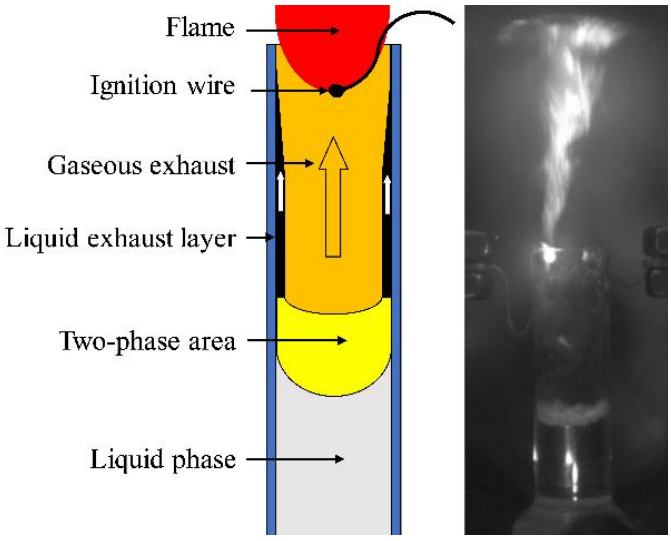

Fig. 11. Combustion structure of 59%HAN-41%[Emim][$EtSO_4$]at 1.0 MPa.

The combustion structure of 59%HAN-41%[Emim][$EtSO_4$] does not fundamentally change with pressure, and is shown and illustrated in Fig. 11. It includes a liquid phase, a two-phase area visible as a white foam where the bulk of HAN decomposition is assumed to happen, and an exhaust area. In the exhaust area, the walls of the propellant holder are covered in a layer of unburned propellant, assumed to be partially decomposed [Emim][$EtSO_4$] entrained by the gaseous exhaust flow. HSI suggests that the propellant undergoes staged combustion, as the exhaust produces a bright flame that is initiated by and emanates from the hot remnant of the ignition wire, as shown in Fig. 11. This behavior is common for high activation energy fuel mixtures reported in the literature. At higher pressure (>2.0 MPa), the end of the combustion is signaled by a rapid descent of the flame down the propellant holder, seen in Fig. 12. At lower pressure (<1.0 MPa) the flame is not observed, and the layer of unburned propellant appears to follow a pulsing vertical movement. The authors hypothesize that the upward entrainment of the exhaust gases is not large enough to counter the weight of the unburned liquid layer, which causes it to fall. When the liquid layer contacts the hot two-phase area, it reacts, causing an increase in gas generation which creates a strong pulse of exhaust gas. This pulse entrains the layer upward, continuing the cycle. Possible causes for this increase in reactivity include decomposition of residual HAN in the falling layer or vaporization of [Emim][$EtSO_4$] decomposition products due to increasing temperature in the two-phase area. The interface between the two-phase area and the liquid area displays a meniscus with a stronger curvature at high burn rate, similar to 80% HAN-water propellant. The radius-to-depth ratio of the meniscus, as defined in Fig. 13, decreases from 1.41 at 1.0 MPa to 1.01 at 2.0 MPa and 0.74 at 10.0 MPa. This interface is corrugated, with a large amount of small-scale instabilities due to bubbling**.**

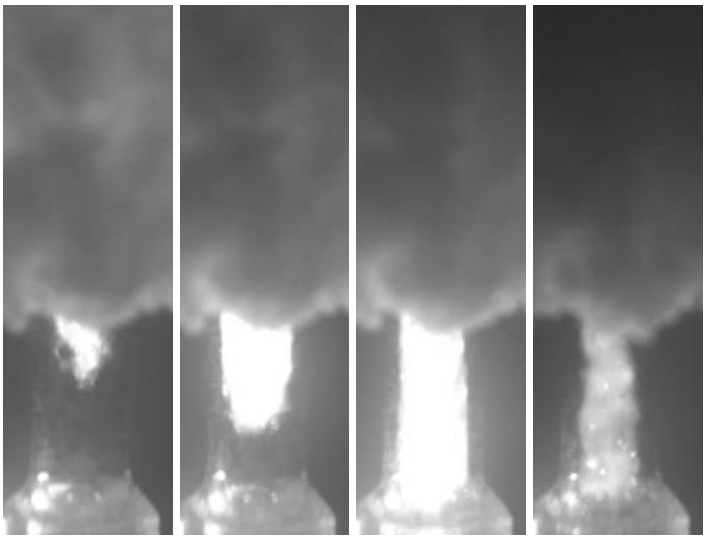

Fig. 12. End of burn flame progression of 59%HAN-41%[Emim][EtSO4] at 8.0 MPa.

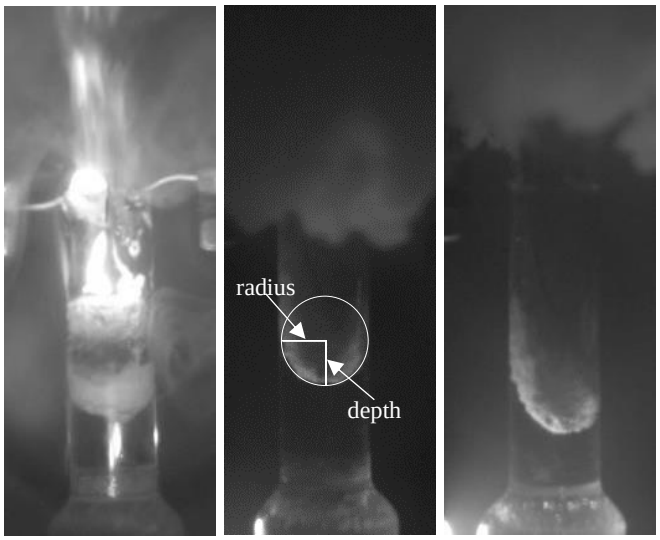

Fig. 13. Two-phase interface at 1.0 MPa, 2.0 MPa and 10.0 MPa (left to right)

CHAPTER 4

DISCUSSIONS

In this section, the results of the current study will be compared with literature. Burn rate and HSI observation of benchmark nitromethane show excellent quantitative agreement with literature data. 80% wt. HAN-water shows a similar pressure trend to the literature data but exhibits a higher burn rate overall. The 59%HAN-41%[Emim][$EtSO_4$] propellant is compared with other HAN-fuel mixtures described in the literature. This propellant is found to have burn rate and visual burning characteristics very similar to other HAN-fuel mixtures. The experimental data points in the following plots are the average of all burn rate measurements for the pressure level considered. The error bars are the 95% confidence interval of the burn rate at that pressure.

4.1 Nitromethane burn rate

Nitromethane linear burn rate has been well-documented in the past. Boyer and Kuo[30] identified a combustion regime in the 3.0-15.0 MPa range in which the linear burn rate exhibits an almost linear relationship with pressure, with further studies confirming these results [27,28,31]. The average linear burn rate measured in this study are plotted in Fig. 14 alongside earlier studies using a similar experimental setup (quartz strand burner). The results show good agreement with previous data. Relative to the least-square linear regression of literature data, the average of HSI-based results over the 3.0 to 11.0 MPa range and the average of pressure-based results in the 3.0 to 9.0 MPa range have respective coefficients of determination of 0.996 and 0.978.

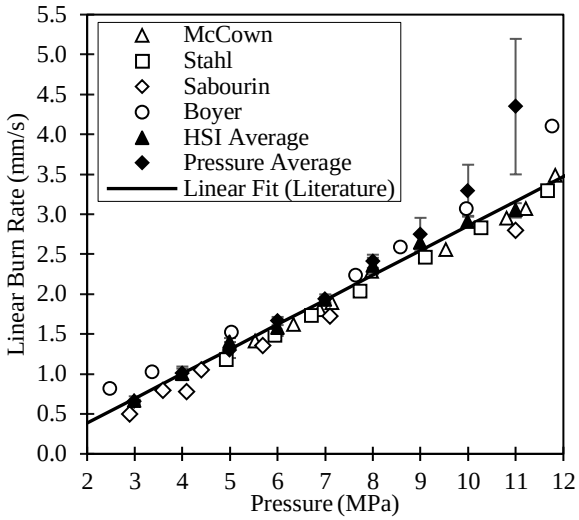

Fig. 14. Comparison of nitromethane linear burn rate with literature results [27,28,30–32]

4.2 80% wt. HAN-water burn rate

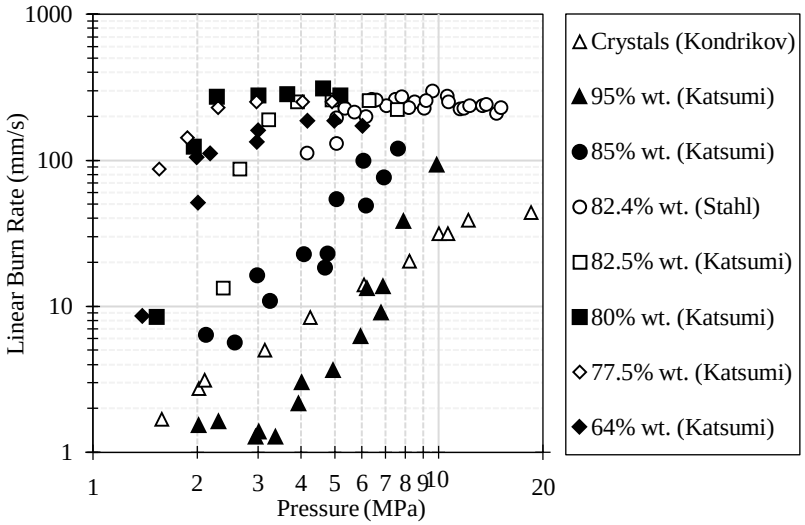

Fig. 15. Literature results for HAN-water linear burn rate [28,29,33]

HAN-water burn rate results from numerous literature sources are provided in Fig. 15. Katsumi [29] found that HAN concentration has an impact on the pressure range at which the transition

occurs and on the maximum burn rate of the propellant. He showed that the burn rate of HAN-water depends primarily on pressure and HAN content, with 3 regions being identified: low burn rate (<10 mm/s), high burn rate (>100 mm/s), and intermediate burn rate. This last region corresponds to the transition between low and high burn rate. For concentrations below 80% wt., the transition is abrupt and takes place between 1 and 3 MPa. Above this limit, the transition takes place over an increasingly larger pressure range, with Kondrikov[33] showing that pure HAN crystals follow a $r_b = aP^n$ law typical of solid propellants in the 1.0-10.0 MPa range. A HAN concentration of 80% wt. corresponds to the maximum linear burn rate, as shown in Fig. 15. In the high burn rate region, the linear burn rate is approximately constant with pressure for all HAN mixtures. This description was confirmed by Stahl [28] in his investigation of the burn rate of 82.4% wt. HAN-water propellant and agrees with the behavior of 80% wt. HAN-water observed in this study. Our results are presented alongside literature data for 80% wt. HAN concentration in Fig. 16.

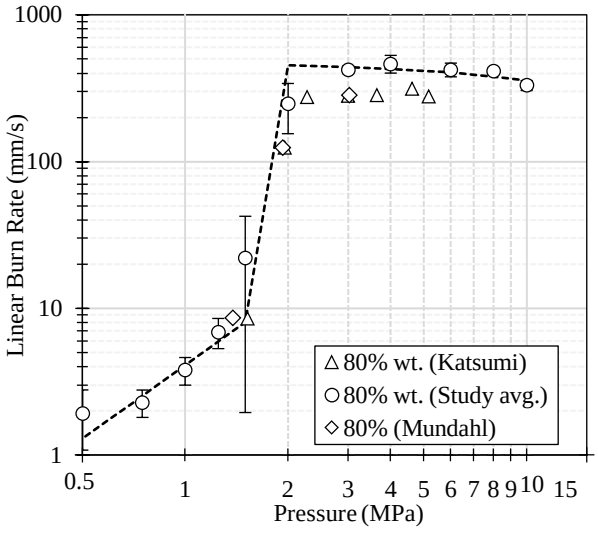

Fig. 16. Comparison of this study's 80% wt. HAN-water burn rate results with literature data [12,34]

While demonstrating transition at the same pressure as previous studies (1.5-2.0 MPa), our measurements suggest a higher linear burn rate above 2.0 MPa. Katsumi reports an average linear burn rate of 288 mm/s between 2.27 and 5.17 MPa while this study found an average of 424 ± 11 mm/s between 3.0 and 6.0 MPa, a 47% increase. This discrepancy is not fully understood. A potential cause could be the use of a propellant holder with a smaller internal diameter (6 mm for this study vs 12 mm for Katsumi), which might cause different hydrodynamic mode to be present during the combustion and thus change the burn rate.

Katsumi developed a useful model for the combustion of HAN-water which explains the link between water content and pressure to the burn rate through the boiling point of the mixture[29]. By acquiring the temperature of the propellant during the burn, it was noticed that in low burn rate mode, the temperature of the exhaust reaches the boiling temperature of water before increasing to a higher value, whereas in high burn rate mode, the temperature of the exhaust stays constant at the boiling temperature of water for the test pressure. The explanation is that in the low burn rate, the decomposition temperature of the mixture is above the boiling point of water, which means that the water boils away during the burn. Because the enthalpy of vaporization of water is high, this effect dominates and effectively slows down the burn rate, as a large proportion of the decomposition energy is expended to vaporize the water. This explains the stratified combustion structure with large bubbles generated at an unsteady rate observed in Fig. 8 for 80% wt. HAN-water at low pressure: the mixture is boiling. Conversely, in the high burn rate mode, the decomposition temperature of the mixture is below or just at the boiling point of water. Because no energy is expended vaporizing water, the burn rate dramatically accelerates through rapid

nucleation of HAN decomposition. This explains the large two-phase area observed at higher pressure in Fig. 8 for 80% wt. HAN-water: the water is not vaporized and a foam of water and HAN decomposition products is formed.

4.3 HAN-fuel mixture burn rate

HAN-fuel mixtures have been extensively studied, first in the context of liquid gun propellant (LGP) research and later as a substitute for hydrazine in space propulsion application. Suitable fuel components, which must be ionic or highly polar to ensure miscibility with HAN, include nitrate salts of aliphatic amines (triethanolammonium nitrate (TEAN)[35] and ethylammonium nitrate (EAN)[33] in particular), zwitterions (amino-acids such as choline[11] and glycine[36]), and alcohols (methanol[34,36]), with water being a frequent additive. Literature results from these studies are presented in Fig. 17 and Fig. 18, and the composition of the literature HAN-fuel propellants given in Table 2. From Fig. 17, in the 1.0-10.0 MPa pressure range, Chang explored the burn rate of XM46 (a mixture of 63.2% wt. HAN, 20% wt. triethanolammonium nitrate (TEAN) and 16.8 % water), first developed as an LGP, as well as HAN-glycine-water (HANGLY26) and HAN-methanol-water mixtures (HAN269MEO15 and HAN284MEO17). Chang found that HAN-based propellant can exhibit staged combustion, particularly with high activation energy fuel such as TEAN [36]. In a staged decomposition, HAN undergoes decomposition first, then TEAN, then the decomposition products react together, creating a bright flame far above the decomposition front of the propellant. In the case of HAN-[Emim][$EtSO_4$], HSI suggests that the propellant also undergoes staged combustion because the exhaust produces a bright flame that appears when initiated by the hot remnant of the ignition wire, as shown in Fig.

11. Chang also reports that a pulsing behavior can be observed in HAN-methanol mixtures under 1.14 MPa[36], similar to the low-pressure behavior of HAN-[Emim][$EtSO_4$] under 1.0 MPa.

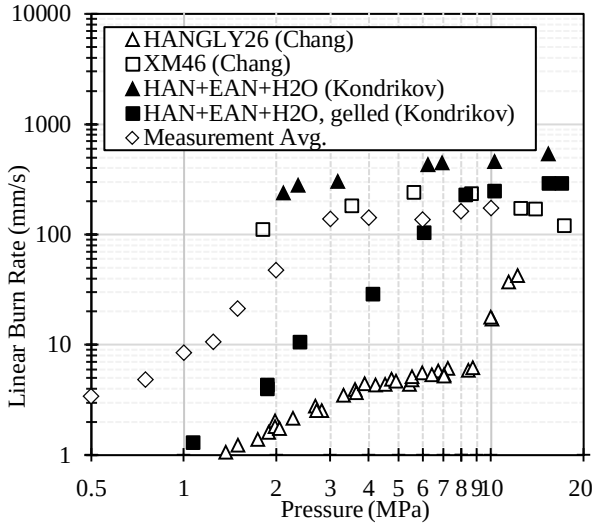

Fig. 17. Comparison of 59%HAN-41%[Emim][$EtSO_4$] propellant linear burn rate with HAN-amine propellants [33,35,36]

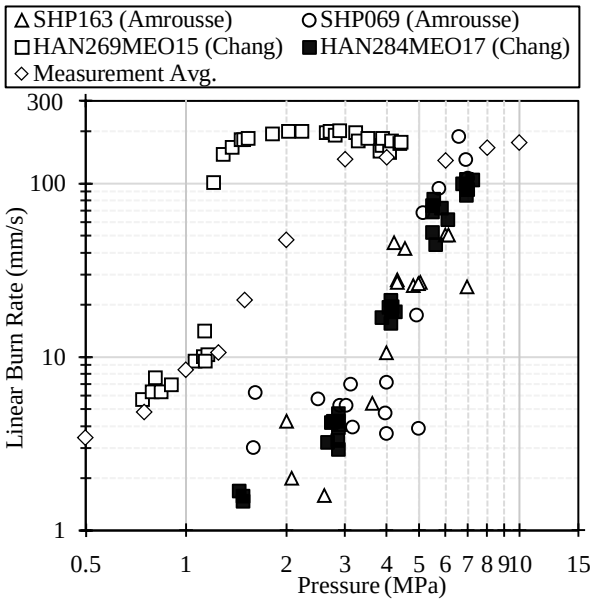

Fig. 18. Comparison of 59%HAN-41%[Emim][$EtSO_4$] propellant linear burn rate with HAN-methanol propellants [34,36].

Methanol has been found to decrease linear burn rate in HAN-fuel mixtures [37], a result confirmed by Amrousse [34]. The lower burn rate of methanol-based propellants can be explained by the boiling point-burn rate model proposed by Katsumi [29] for HAN-water mixture because methanol lowers the boiling temperature of the propellant [37]. A lower boiling temperature means that the propellant will stay in the low burn rate mode over a wider pressure range, delaying the transition to high burn rate. The comparison of the burn rates of HAN269MEO15 (14.91% water, 15.39% methanol) and HAN284MEO17 (4.86% water, 17.86% methanol) in Fig. 18 clearly demonstrate the transition-delaying effect of a higher methanol-to-water content.

The burn rate of HAN with ethanolammonium nitrate (EAN), a room-temperature ionic liquid, has been reported by Kondrikov [33] both in gelled and conventional liquid form. A significantly higher burn rate is observed for non-gelled propellant, which indicates that hydrodynamic effects have a strong influence on burn rate. In addition, it is observed that the propellants with the highest water content (notably HAN269MEO15 and HANGLY26) have the most abrupt transitions from low to high burn rate. Comparing propellant composition in Table 2 with the burn rate trends of Fig. 17 and Fig. 18 indicates that higher water content gives rise to more abrupt transition from low to high burn rate. In contrast, low-water (<10%) propellants do not have obvious discontinuities in their burn rate vs. pressure, exhibiting a wide transition zone. This is similar to the behavior observed in HAN-water solution (Fig. 15), with the more dilute mixtures have more abrupt transitions than concentrated ones. The burn rate of HAN-[Emim][$EtSO_4$] is presented in Fig. 17 and Fig. 18 along with the literature results for other HAN-fuel propellants. The smooth low-to-high burn rate is consistent with the absence of water in its composition. The range and trend of burn rates measured here (1-200 mm/s) are similar to those of other HAN-fuel mixtures.

Table 2. Literature Propellant Composition

Propellant	Water content (%)	HAN Content (%)	Fuel Content (%)	Fuel Species
HANGLY26	26	60	14	Glycine
XM46	16.8	63.2	20	TEAN
HAN269MEO15	14.91	69.7	15.39	Methanol
SHP069	6.9	81.9	11.21	Methanol
SHP163	6.20	73.64	20.16	Methanol
Kondrikov	5	57.5	37.5	EAN
HAN284MEO17	4.89	77.25	17.86	Methanol

CHAPTER 5

CONCLUSION

The linear burn rates of nitromethane, 80% wt. HAN-water, and 59%HAN-41%[Emim][$EtSO_4$] have been measured and their combustion behavior documented through high-speed imaging. The results obtained for nitromethane agree well with the literature with a coefficient of determination above 0.97, while 80% wt. HAN-water shows combustion behavior and burn rate trends similar to previous studies, albeit with a consistently higher burn rate. In particular, it is found that 80% wt. HAN-water burn rate follows a power law $r_b = 4.09P^{1.66}$ between 0.5 and 1.5 MPa and a linear law $r_b = 478 - 12.30P$ between 2.0 and 10.0 MPa. The combustion structure of 59%HAN-41%[Emim][$EtSO_4$] is characterized by a liquid phase, two-phase area, and an exhaust area including a liquid film layer of unburned propellant and a stream of hot decomposition gases undergoing staged combustion. Its burn rate follows an exponential law $r_b = 5.35e^{1.11P}$ between 0.5 and 3.0 MPa and a linear law $r_b = 114 + 3.84P$ between 3.0 and 10.0 MPa. These results show behavior that is similar to other HAN-fuel mixtures previously studied in the literature. A large variability in the low-pressure linear burn rate was observed with a maximum margin of error of 54% at 0.5 MPa. Further study of HAN-ionic liquid monopropellants is needed to characterize the influence of ionic liquid properties and proportions on burn rate, and offer a suitable model for their combustion. The temperatures in the two-phase and gas-phase regions, and analysis of the composition of unburned propellant, would be useful in characterizing the thermochemical behavior of the propellant. The influence of preparatory routes on HAN-ionic liquid combustion behavior should also be investigated.

REFERENCES

[1] C.A. Kluever, Spacecraft optimization with combined chemical-electric propulsion, J. Spacecr. Rockets 32 (1995) 378–380.

[2] C.A. Kluever, Optimal geostationary orbit transfers using onboard chemical-electric propulsion, J. Spacecr. Rockets 49 (2012) 1174–1182.

[3] S.R. Oleson, R.M. Myers, C.A. Kluever, J.P. Riehl, F.M. Curran, Advanced propulsion for geostationary orbit insertion and north-south station keeping, J. Spacecr. Rockets 34 (1997) 22–28.

[4] T. Rexius, M. Holmes, Mission capability gains from multi-mode propulsion thrust profile variations for a plane change maneuver, AIAA Modeling and Simulation Technologies Conference 2011 (2011), pp. 567–580.

[5] S.P. Berg, J.L. Rovey, Assessment of multimode spacecraft micropropulsion systems, J. Spacecr. Rockets 54 (2017) 592–601.

[6] B.R. Donius, J.L. Rovey, Ionic liquid dual-mode spacecraft propulsion assessment, J. Spacecr. Rockets 48 (2011) 110–123.

[7] S.P. Berg, J.L. Rovey, Assessment of imidazole-based ionic liquids as dual-mode spacecraft propellants, J. Propuls. Power 29 (2013) 339–351.

[8] S.P. Berg, J.L. Rovey, B.D. Prince, S.W. Miller, R.J. Bemish, Electrospray of an energetic ionic liquid monopropellant for multi-mode micropropulsion applications, 51st

AIAA/SAE/ASEE Joint Propulsion Conference (2015).

[9] Y.C. Chao, G.B. Chen, C.J. Hsu, T.S. Leu, C.Y. Wu, T.S. Cheng, Operational characteristics of catalytic combustion in a platinum microtube, Combust. Sci. Technol. 176 (2004) 1755–1777.

[10] F.G. Kidd, N.R. Taylor, K.M. Lemmer, Decomposition of hydroxylammonium nitrate in a low pressure flowing thermal capillary system, J. Mol. Liq. 262 (2018) 396–404.

[11] A.J. Mundahl, S.P. Berg, J.L. Rovey, M. Huang, K. Woelk, D. V. Wagle, G. Baker, Characterization of a novel ionic liquid monopropellant for multi-mode propulsion, 53rd AIAA/SAE/ASEE Joint Propulsion Conference (2017), pp. 1–20.

[12] A.J. Mundahl, S.P. Berg, J.L. Rovey, Linear burn rate of monopropellant for multi-mode micropropulsion, 2018 Joint Propulsion Conference (2018), pp.1–11.

[13] V. Hruby, M. Gamero-Castaño, P. Falkos, S. Shenoy, Micro Newton colloid thruster system development, 27th International Electric Propulsion Conference (2001), pp. 01–281.

[14] D. Spence, E. Ehrbar, N. Rosenblad, N. Demmons, T. Roy, S. Hoffman, D. Williams, M. Tsay, J. Zwahlen, K. Hohman, V. Hruby, C. Tocci, Electrospray propulsion systems for small satellites and satlets, AIAA Space Conference and Exposition 2013 (2013), pp. 1–7.

[15] Y.H. Chiu, R.A. Dressler, Ionic liquids for space propulsion, ACS Symposium Series 975 (2007), pp. 138–160.

[16] S.P. Berg, J.L. Rovey, Decomposition of double salt ionic liquid monopropellant in a

microtube for multi-mode micropropulsion applications, 53rd AIAA/SAE/ASEE Joint Propulsion Conference (2017).

[17] R.L. Sackheim, R.K. Masse, Green propulsion advancement: Challenging the maturity of monopropellant hydrazine, J. Propuls. Power 30 (2014) 265–276.

[18] A.S. Gohardani, J. Stanojev, A. Demairé, K. Anflo, M. Persson, N. Wingborg, C. Nilsson, Green space propulsion: Opportunities and prospects, Prog. Aerosp. Sci. 71 (2014) 128–149.

[19] G.P. Sutton, O. Biblarz, Rocket Propulsion Elements 7th, Wiley, New York, USA, 2001.

[20] L. Courthéoux, D. Amariei, S. Rossignol, C. Kappenstein, Thermal and catalytic decomposition of HNF and HAN liquid ionic as propellants, Appl. Catal. B Environ. (2006) 217–225.

[21] K. Anflo, R. Möllerberg, Flight demonstration of new thruster and green propellant technology on the PRISMA satellite, Acta Astronaut. 65 (2009) 1238–1249.

[22] M. Farshchi, V. Vaezi, B.D. Shaw, Studies of Han-based monopropellant droplet combustion, Combust. Sci. Technol. 174 (2002) 71–97.

[23] N. Wingborg, C. Eldsäter, H. Skifs, Formulation and characterization of ADN-based liquid monopropellants, European Space Agency Special Publication (2004) 101–106.

[24] R. Masse, R.A. Spores, S. Kimbrel, M. Allen, E. Lorimor, P. Myers, C. McLean, GPIMAF-M315E propulsion system, 51st AIAA/SAE/ASEE Joint Propulsion Conference (2015), pp.

1–10.

[25] K. Anflo, B. Crowe, In-space demonstration of an ADN-based propulsion system, 47th AIAA/ASME/SAE/ASEE Joint Propulsion Conference and Exhibit (2011), pp. 1–14

[26] W.C. Warren, E.L. Petersen, Experimental Techniques for the Study of Liquid Monopropellant Combustion, Master's Thesis, Texas A&M University, College Station, TX, USA, 2012.

[27] K.W. McCown, A.R. Demko, E.L. Petersen, Experimental techniques to study linear burning rates of heterogeneous liquid monopropellants, J. Propuls. Power 30 (2014) 1027–1037.

[28] J. Mac Stahl, E.L. Petersen, Analysis of Hydroxylammonium Nitrate Burning Rates, Master's Thesis, Texas A&M University, College Station, TX, USA, 2017.

[29] T. Katsumi, K. Hori, R. Matsuda, T. Inoue, Combustion Wave Structure of Hydroxylammonium Nitrate Aqueous Solutions, 46th AIAA/ASME/SAE/ASEE Joint Propulsion Conference & Exhibit (2010).

[30] E. Boyer, K.K. Kuo, High-pressure combustion behavior of nitromethane, 35th Joint Propulsion Conference & Exhibit (1999).

[31] J.L. Sabourin, R.A. Yetter, V.S. Parimi, Exploring the effects of nanostructured particles on liquid nitromethane combustion, J. Propuls. Power. 26 (2010) 1006–1015.

[32] S. Kelzenberg, N. Eisenreich, W. Eckl, V. Weiser, Modelling Nitromethane Combustion,

Propellants, Explos. Pyrotech. 24 (1999) 189–194.

[33] B.N. Kondrikov, V.E. Annikov, V.Y. Egorshev, L.T. De Luca, Burning of hydroxylammonium nitrate, Combust. Explos. Shock Waves 36 (2000) 135–145.

[34] R. Amrousse, T. Katsumi, N. Azuma, K. Hori, Hydroxylammonium nitrate (HAN)-based green propellant as alternative energy resource for potential hydrazine substitution: From lab scale to pilot plant scale-up, Combust. Flame 176 (2017) 334–348.

[35] Y.P. Chang, E. Boyer, K.K. Kuo, Combustion behavior and flame structure of XM46 liquid propellant, J. Propuls. Power 17 (2001) 800–808.

[36] Y.-P. Chang, Combustion Behavior of HAN-Based Liquid Propellants, Doctoral Thesis, The Pennsylvania State University, University Park, PA, USA, 2002.

[37] Y.P. Chang, J.K. Josten, B.Q. Zhang, K.K. Kuo, B.D. Reed, Combustion characteristics of energetic HAN/Methanol-based monopropellants, 38th AIAA/ASME/SAE/ASEE Joint Propulsion Conference and Exhibit (2002).

APPENDIX

PROPELLANT PREPARATION METHOD

PART 1

[EMIM][ETSO$_4$] PURIFICATION

1.1 Background and justification

The [Emim][EtSO$_4$] used to prepare propellant in the Electric Propulsion Laboratory is sourced from Sigma-Aldrich. It is packaged in 100g bottles and has a purity above 95%. The purpose of the purification step is to remove volatile impurities of the liquid, notably precursor remnants diethyl sulfate and 1-methylimidazole (which cause the pungent smell of [Emim][EtSO$_4$]), and water. These impurities can negatively affect the performance of the propellant in both electric and chemical mode. Previous studies exposed the ionic liquid to high vacuum (<mTorr) at room temperature (20°C) to perform this purification step. Water content measurement of [Emim][EtSO$_4$] prepared using this process were performed using a Hanna Instrument HI904 Karl-Fischer titrator, which showed small to no change in water content compared to [Emim][EtSO$_4$] freshly sampled out of the bottle. The smell of [Emim][EtSO$_4$] disappeared, indicating a reduction in volatile impurities. Consequently, an improved method for purification was devised using a rotary evaporator, which uses a conjunction of heat, vacuum, and agitation to increase the evaporation rate.

The extremely hygroscopic nature of the ionic liquid motivated the use of air-free handling techniques, which allow us to consistently reach a water content in [Emim][$EtSO_4$] under 100 ppm.

1.2 Pressure circuit controls

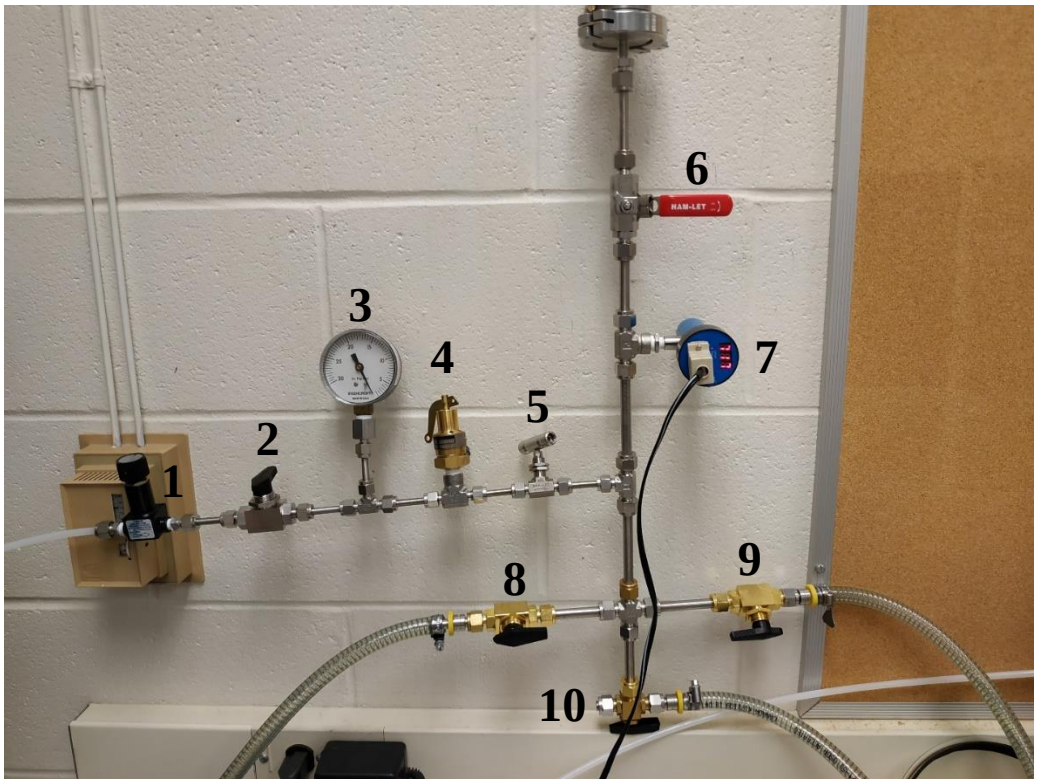

1. Pressure regulator
2. Dry air valve
3. Dry air pressure gauge
4. Dry air pressure relief valve
5. Adjustable dry air needle valve
6. Vacuum valve
7. Vacuum gauge
8. Rotary evaporator valve

9. 24/40 adapter valve
10. Dessicator valve

1.3 Material list

Personal Protective Equipment

1. Laboratory coat, preferably fire-resistant
2. Nitrile gloves
3. Goggles or face shield
4. Closed-toe shoes and long pants

Processing material

5. Rotary evaporator

6. 2-neck round bottom flask with 24/40 ground glass joints, choose size for desired quantity.
7. 24/40 Rubber septum
8. 24/40 tap adapter

9. Cork stand for the round bottom flask

10. Scale with maximum capacity > 300 g and precision <0.1 g

11. 5 mL or larger syringe with Luer lock tip (“transfer syringe”)

12. 20 gauge 4 in long Luer lock needle

13. 100 mL beaker for waste

Consumables

14. Distilled water (1 to 2 gallons)

15. [Emim][$EtSO_4$] bottle equipped with septum cap

16. Vacuum grease

Cleaning material

17. Isopropyl alcohol

18. Laboratory oven

19. Dessicator

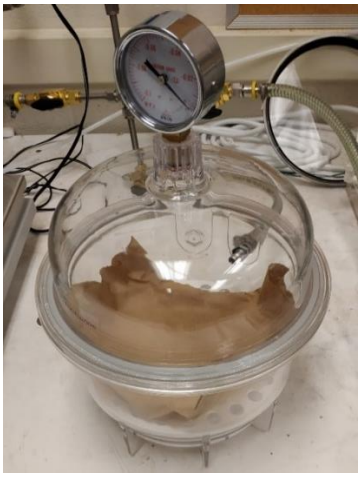

20. Ultrasonic cleaner

21. tongs or heat-resistant gloves

Titration material

22. HI-904 Karl-Fischer titrator with Hydranal Coulomat AG-H reagent

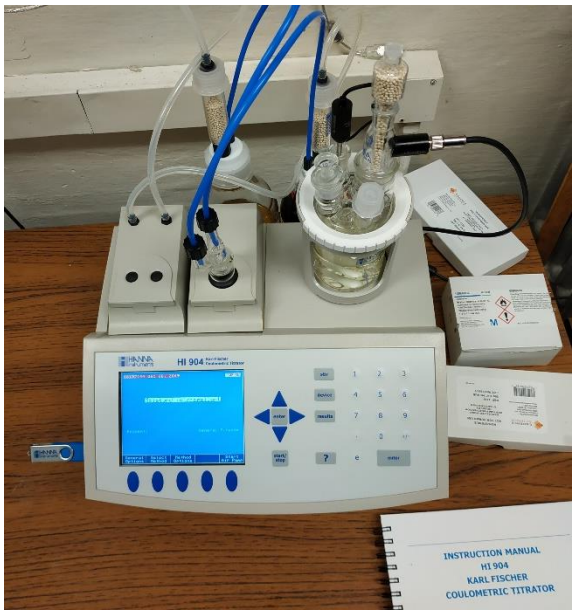

23. 1 mL syringe with Luer lock tip (“titration syringe”)

24. 20 gauge 6 in long Luer lock needle

1.4 Glassware preparation

Prior to the purification process, the glassware coming in direct contact with [Emim][$EtSO_4$] must be cleaned and dried to prevent cross-contamination.

1. Ultrasonic cleaning of the glassware at 50°C for 30 minutes in distilled water+dishwasher soap solution.
2. Thorough washing of the glassware with distilled water first, to remove soap residues, followed by a thorough washing with isopropyl alcohol.
3. Leave the glassware to dry for an hour in the dessicator under 1 Torr.
4. Preheat the oven to 110 °C and store the glassware in the oven for at least 6 hours. Alternatively, if no oven is available, the glassware can be washed with acetone. However, this method will leave a larger amount of residual water.
5. Using tongs or heat-resistant gloves, transfer the glassware to the dessicator and allow it to cool under vacuum for 1 hour or until it is safe to touch.

1.5 Purification process

All [Emim][$EtSO_4$] handling should take place in the glove box under less than 0.5% relative humidity to minimize water intake from the atmosphere. Outside of the glove box, the [Emim][$EtSO_4$] must be transferred in a sealed container, such as the round bottom flask with septum installed and tap closed.

1. Fill the bath of the evaporator with distilled water and set its temperature to 60°C.
2. Spread a thin layer of grease on the male joint of the tap adapter. Connect the central round bottom flask joint to the tap male joint. Rotate the joint to spread the grease. The tap should be in the closed position. Install the septum on the side joint.
3. Record the weights of the cork stand, then of the flask assembly using the scale.

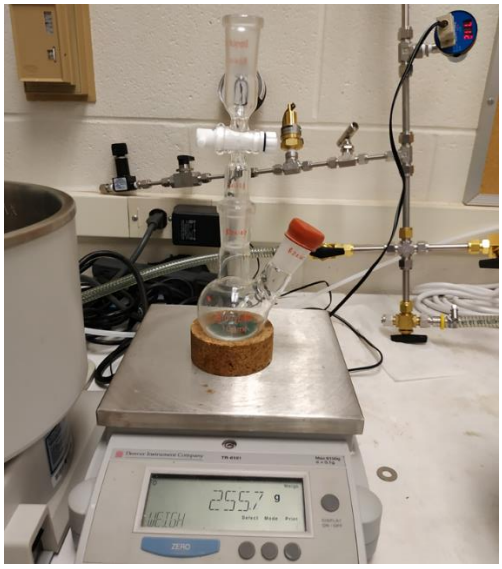

4. Tare the scale for the flask assembly resting on the cork stand.
5. Equip the transfer syringe with a 4 in needle and rinse at least twice by sampling 1-2 mL from the [Emim][$EtSO_4$] bottle through the septum, coating the internal surface of the syringe thoroughly, and eliminating the waste in the beaker.
6. Fill the syringe entirely with [Emim][$EtSO_4$] and transfer it in the round bottom flask through the septum. Repeat until the mass of ionic liquid reaches the desired target. Dispose of any excess in the waste beaker.
7. Titrate the [Emim][$EtSO_4$] using the titration syringe equipped with the 6 in needle and the "water in propellant" titrator method. Follow the procedure described in the HI 904 manual at

page 6-7. Repeat this procedure three time to allow the calculation of an average water content with margin of error.

8. Grease the rotary evaporator joint and connect the flask assembly. Open the tap and start pulling a vacuum in the evaporator. The vacuum level should be under 1 Torr.

9. Lower the flask into the bath and start the rotation. The septum should not touch the water directly. Adjust the angle and vertical position to avoid splashing.
10. Leave the [Emim][$EtSO_4$] to dry for 2 hours. If necessary, add distilled water to the bath to avoid exposing the resistors to air.
11. When the drying is finished, stop the rotation and elevate the vial out of the bath. Slowly repressurize the evaporator using dry air. When the pressure reaches 600 Torr, stop the flow of dry air and open one of the relief valves to equalize the pressure.
12. Close the tap on the round bottom flask and disconnect it from the evaporator. Wipe it to remove any residual water and weight the flask to determine the mass loss during the drying process.

13. Titrate the [Emim][$EtSO_4$] following the same procedure as in step 7. The [Emim][$EtSO_4$] is considered pure enough for propellant application when the water content is below 150 ppm. If the water content is above this limit, repeat the procedure starting from step 8.
14. Store the propellant in the dry box in a sealed container, either by keeping it in the round bottom flask assembly or by transferring it in a septum-capped vial using the transfer syringe.
15. Rinse all glassware which encountered [Emim][$EtSO_4$] with distilled water and IPA.

PART 2

HYDROXYLAMMONIUM NITRATE DRYING PROCESS

2.1 Background and justification

The hydroxylammonium nitrate (HAN) used to prepare propellant in the Electric Propulsion Laboratory is sourced from Sigma-Aldrich. It is packaged in 500 mL bottles as an aqueous solution containing 24% wt. HAN with a purity above 99.999%. Water is undesirable in the propellant; it is necessary to dry the HAN until it crystallizes as a white solid, which will be dissolved in the ionic liquid.

The extraction procedure is divided in two steps. First, the 24% wt. aqueous solution is concentrated to >90% using the rotary evaporator. Above this limit, water evaporation slows down significantly and requires high temperatures (>70°C) to proceed, which increases the risk of HAN decomposition. The second step consists of an azeotropic distillation using a water/isopropyl alcohol (IPA) mixture containing less than 12% water by mass. In this configuration, water is selectively evaporated from the liquid mixture until the liquid phase theoretically contains only IPA and HAN. Because the solubility of HAN in IPA is low, it crystallizes rapidly. The process is continued until all the IPA and water has been evaporated. In practice, due to the extreme hygroscopicity of HAN, the current procedure cannot produce crystals containing less than 2% water. For this reason, HAN crystals should be handled with air-free techniques similar to those used for [Emim][$EtSO_4$].

IMPORTANT NOTE: The maximum amount of HAN that we have dried to solid crystalline form in a single batch to date is 30 g. Larger batches have not been investigated, may be unstable, and should not be pursued at this time.

2.2 Material list

Personal Protective Equipment

1. Laboratory coat, preferably fire-resistant
2. Nitrile gloves
3. Goggles or face shield
4. Closed-toe shoes and long pants

Processing material

5. Rotary evaporator
6. 2-neck round bottom flask with 24/40 ground glass joints, choose size for desired liquid quantity
7. 24/40 Rubber septum
8. 24/40 tap adapter
9. Cork stand for the round bottom flask
10. Scale with maximum capacity > 300 g and precision <0.1 g
11. Nucleation rod (glass rod with a sanded end)

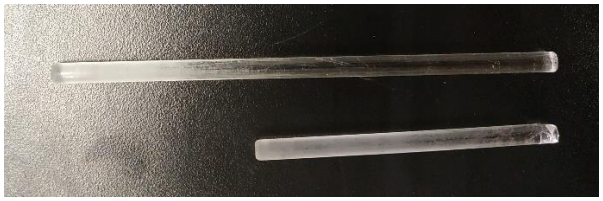

12. Glass rod

13. Clamp stand

Consumables

14. Distilled water (1 to 2 gallons)

15. 24% wt. HAN-water solution, Sigma-Aldrich no. 438235

16. Isopropyl alcohol (IPA)

17. Vacuum grease

Cleaning material

18. Laboratory oven

19. Dessicator

20. Ultrasonic cleaner

21. tongs or heat-resistant gloves

2.3 HAN Drying process

Prior to this procedure, all glassware should be cleaned and dried following the procedure presented in section 1.3.

1. Go to the Sigma-Aldrich webpage for the HAN-water solution and pull the certificate of analysis (COA) for the lot number reported on the HAN-water bottle. Record the actual HAN content of the solution.

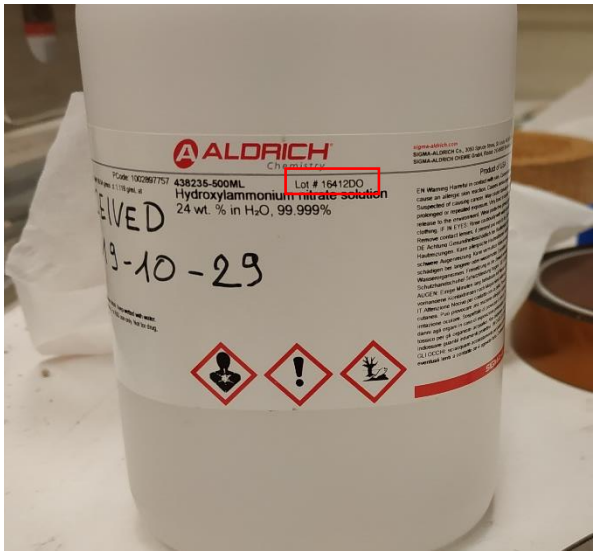

2. Fill the bath of the evaporator with distilled water and set its temperature to 50°C.
3. Spread a thin layer of grease on the male joint of the tap adapter. Connect the central round bottom flask joint to the tap male joint. Rotate the joint to spread the grease. The tap should be in the closed position. The side neck should be open.
4. Record the weights of the cork stand, then of the flask assembly using the scale.
5. Tare the scale for the flask assembly resting on the cork stand.
6. Fill the flask with the desired amount of HAN solution through the side neck and record the weight of the solution. Install the septum on the side neck of the flask.
7. Grease the rotary evaporator joint and connect the flask assembly. Open the tap and start pulling a vacuum in the evaporator; the liquid should start to boil vigorously.
8. Lower the flask into the bath and start the rotation. The septum should not touch the water directly. Adjust the rotation to avoid splashing.
9. Let the evaporation proceed for 30 minutes. The pressure gauge should read less than one Torr and any boiling should have stopped.

10. Stop the rotation and elevate the vial out of the bath. Slowly repressurize the evaporator using dry air. When the pressure reaches 600 Torr, stop the flow of dry air and open one of the relief valves to equalize the pressure.
11. Close the tap on the round bottom flask and disconnect it from the evaporator. Wipe it to remove any residual water and weight the flask to determine the mass loss incurred during the concentration process. The mass should correspond to a water content less than 10%. Else, repeat the procedure starting from step 6.
12. Record the weight of the nucleation rod. Remove the septum and insert it in the flask.
13. Add IPA so that the mass of liquid (IPA+HAN+water) is equal or above the starting mass of solution, prior to the evaporation. Record the mass of IPA added. Reinstall the septum.
14. Set the flask on the clamp stand and connect it to the vacuum line through the tap joint.

15. Start pulling vacuum at a moderate rate by adjusting the position of the vacuum valve. The pressure should be around 15 Torr. This is necessary to avoid explosive boiling in the flask.

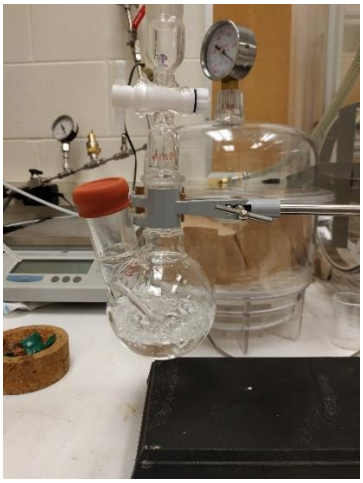

16. If crystallization starts or if boiling stops, fully open the vacuum valve.
17. Leave the HAN to crystallize for at least 12 hours.
18. Confirm that the crystals are white and dry. Repressurize slowly the round bottom flask until the pressure reaches 600 Torr, then stop the flow of dry air and open one of the relief valves to equalize the pressure. Close the tap and disconnect the flask assembly.
19. Measure the weight of HAN crystals. Using the HAN content in the initial mass of solution, calculate the humidity of the crystals.
20. In the glove box, remove the septum and gently dislodge the crystals from the walls of the flask using the glass rod and break them down to pieces small enough to fit through the neck of the flask.
21. The HAN crystals should be stored in the glove box in a sealed container for as short of a time as possible, owing to their extreme hygroscopicity and reported instability.

PART 3

PROPELLANT MIXING PROCESS

3.1 Background and justification

Because [Emim][$EtSO_4$] is a viscous liquid and the current propellant mixture ratio is close to the maximum solubility of HAN in [Emim][$EtSO_4$], a very vigorous mixing procedure is thus necessary to dissolve the crystals. In addition, the crystals themselves are porous. These effects tend to inject a large quantity of bubbles in the mixture, which means that the propellant must be vacuum degassed prior to storage and use. There is currently no known way to reduce humidity in the mixed propellant; it is therefore necessary to keep it in a sealed container at all time.

IMPORTANT NOTE: The maximum amount of [Emim][EtSO4]-HAN propellant that we have mixed and synthesized in a single batch to date is 50 g (38 mL). Larger batches have not been investigated, may be unstable, and should not be pursued at this time.

3.2 Material list

Personal Protective Equipment

1. Laboratory coat, preferably fire-resistant
2. Nitrile gloves
3. Goggles or face shield
4. Closed-toe shoes and long pants

Processing material

5. 2-neck round bottom flask with 24/40 ground glass joints, adapt for desired liquid quantity
6. 24/40 Rubber septum

7. 24/40 tap adapter
8. Cork stand for the round bottom flask
9. Beaker, adapt size and number for propellant quantity
10. Glass rod, 12 inches, fire polished if possible
11. Vial with rubber septum cap, adapt size and number for propellant quantity
12. Funnel
13. 5 mL or larger syringe with Luer lock tip (“transfer syringe”)
14. 20 gauge 4 in long Luer lock needle
15. High precision scale (±1 mg at least)
16. Waste beaker

Consumables

17. HAN crystals
18. Purified [Emim][$EtSO_4$]
19. Vacuum grease

Titration material

20. HI-904 KF titrator with associated accessories
21. 1 mL syringe with Luer lock tip (“titration syringe”)
22. 20 gauge 6 in long Luer lock needle

3.3 Mixing procedure

Prior to the operation, all glassware should be cleaned and dried following the procedure presented in section 1.3.

1. In the glove box, tare the scale for the beaker weight.

2. Using the funnel and glass rod if necessary, introduce the HAN crystals in the beaker. Record the weight and calculate the amount of [Emim][$EtSO_4$] required to reach the O/F ratio of the propellant (59% HAN and 41% [Emim][$EtSO_4$] for the standard formulation)
3. Assemble the transfer syringe with its needle and rinse it twice with [Emim][$EtSO_4$]. Then, transfer [Emim][$EtSO_4$] in the beaker drop by drop, monitoring the weight to reach the desired amount as closely as possible.
4. Stir the beaker with the glass rod until most of the HAN is dissolved in the [Emim][$EtSO_4$].
5. Using the funnel, transfer the propellant to the round bottom flask.Equip the round bottom flask with the greased tap assembly and the septum. Use the glass rod to scrape the undissolved flakes of HAN into the flask.
6. Close the tap and connect the round bottom flask to the vacuum circuit. Pull a vacuum over the propellant until all bubbles and HAN fragments have disappeared.

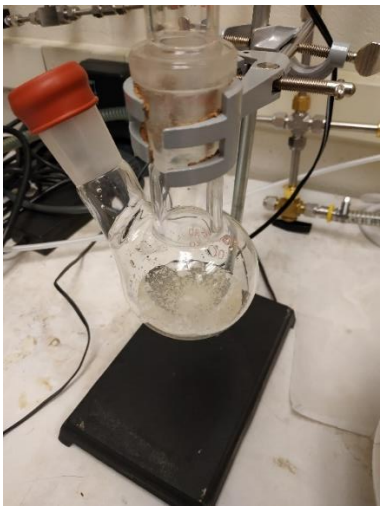

7. Slowly repressurize the flask using dry air. When the pressure reaches 600 Torr, stop the flow of dry air and open one of the relief valves to equalize the pressure.
8. Close the tap and transfer the flask in the dry box for storage.